DOI: 10.18462/iir.gl2022.0155

Coupled Fluid-Solid Modelling of the Valve Dynamics in Reciprocating Compressors

Åsmund ERVIK* [(a)], Afaf SAAI[(b)], Torodd BERSTAD[(c)], Ole MEYER[(a)], Takuma TSUJI[(d)], Tatsuya OKU[(d)], Kazuhiro HATTORI[(d)], Kazuya YAMADA[(d)], Virgile DELHAYE[(b)], Petter NEKSÅ[(a)]

[(a)] SINTEF Energy Research, 7034 Trondheim, Norway
[(b)] SINTEF Industry, 7034 Trondheim, Norway
[(c)] Norwegian University of Science and Technology, 7034 Trondheim, Norway
[(d)] Mayekawa MFG Co., LTD., Botan Koto ku, Tokyo, Japan
*Corresponding author: asmund.ervik@sintef.no

ABSTRACT

A novel method coupling computational fluid dynamics (CFD) and finite element method (FEM) was developed to account for the complex physics of the reciprocating compressor. The developed method is based on data exchange between the two solvers at each time step. We address the challenges related to valve dynamics, where the motion of solid components is not prescribed as for pistons, but result from the combined interactions between pressure, velocity, spring forces and impact forces during each revolution. The coupling method enables accurate computation of the solid-fluid interaction, where at each time step the pressure acting on the valve computed by CFD is transferred to the FEM simulation, and the three-dimensional valve motion computed by FEM is transferred to the CFD simulation. It is demonstrated on the dynamics of a ring plate discharge valve in a reciprocating ammonia compressor to quantify the effect of impact damping which arises from the gas dynamics, leading to reduced forces on the valve. The results from the coupling simulations are compared against novel experimental measurements obtained by instrumenting a real compressor. The coupled CFD-FEM simulation gives detailed insights into the valve behaviour and was used also to investigate pressure inhomogeneities, which can lead to tumbling motion of the valve ring.

Keywords: Reciprocating compressor, Ring plate valves, Valve dynamics, CFD, FEM, Experiments.

1. INTRODUCTION

Compressors are the driving force of refrigeration systems, providing the circulation of refrigerant, the increase in pressure and thus the transport of heat from the cold to the hot side. The reciprocating compressor (Figure 1) is the best choice for medium capacity systems and has been the topic of many studies since Lorentzen (1950). The compressor needs to meet strict requirements of high capacity, flexibility and efficiency, together with low cost and high reliability. But refrigeration systems must also comply with environmental regulations including the Montreal Protocol and the subsequent Kigali Amendment, meaning that working fluids should have benign effects on the ozone layer and global warming. The natural working fluids provide an obvious solution to this combination of constraints. Here we consider ammonia-based systems, see reviews e.g. by Palm (2008) and Pearson (2008). In the reciprocating compressor one must incorporate valves to allow the piston to alternate between the suction and discharge parts of the stroke. Of these we consider the discharge valve, which faces the harshest conditions as it is actuated by the high-pressure gas that has been compressed in the cylinder. We will focus here on the ring plate valve, where a ring is made to cover an annular hole. Its motion is controlled by springs and the pressure difference between the cylinder and the discharge chamber. The preloaded springs act to keep the valve closed until the pressure differential from cylinder to discharge chamber is large enough to overcome the spring force, lift the valve ring, and the compressed gas can be discharged, as shown in Figure 1.

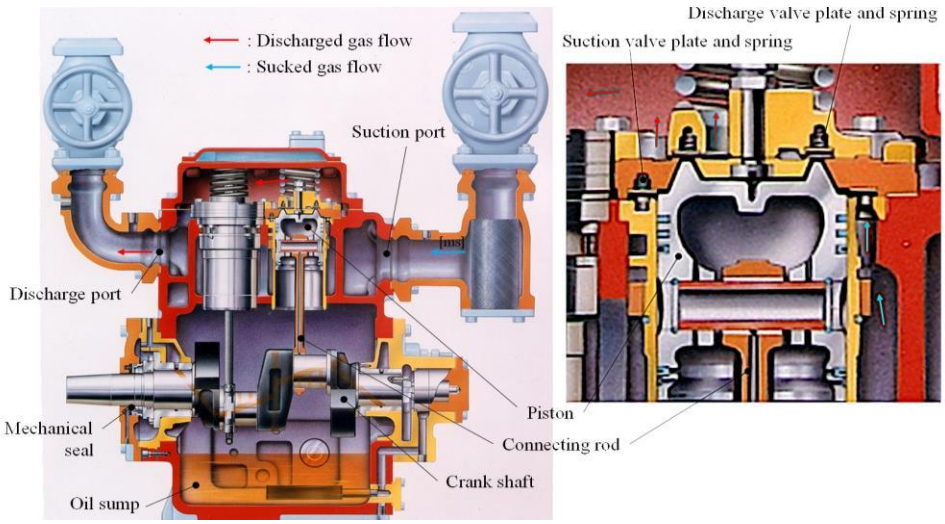

Figure 1:Illustration of the piston compressor and valves

Although the valve dynamics have been a focus of study for decades, there remains much to explore due to the high complexity of the system. The first works were based on experimental or one-dimensional numerical techniques, e.g., Adams et al. (1974), Bredesen (1974), Elson and Soedel (1974). CFD computations of the flow through valves has been undertaken previously (e.g., Cyklis, 1994; Habing, 2005; Ruman et al., 2015; Zhao et al., 2018), and for the case of reed valves there have been investigations using combined FEM and CFD modelling (Kim et al., 2008, Tan et al., 2014, Tofique et al., 2021). In previous work (Ervik et al., 2021) we employed loosely coupled CFD-FEM simulations, where the pressure computed was first computed by CFD and then used as input in the FEM to study ring plate valve dynamics. In the present work we have extended this to tightly coupled CFD-FEM computations based on incremental interaction between CFD and FEM during the real-time of process modelling. The new coupling method will be described in the first section of the paper. The second section reports quantitative measurements obtained by instrumenting Mycom M-series compressor with ammonia refrigerant at representative conditions. The effects of the flow in the cylinder, the contact damping and the pressure inhomogeneity on the valve dynamic as predicated CFD-FEM simulations are discussed and compared to experimental measurement in the second section.

2. COMPUTATIONAL METHODS

The computational modelling employed here consists of FE model and CFD model that have been tightly coupled by exchanging data between the two codes at the end of each timestep. The exchanged data are subsequently used in each code as boundary conditions when computing the solution at the next timestep. The detailed description of the FE model, the CFD model and their coupling strategy are detailed in the next sections.

2.1. Finite Element Modelling (FEM)

The FE analysis is performed using LS-DYNA (Livermore Software Technology, version R10.1.0). Figure 2 shows the assembly of the discharge valve as represented by the FE model. It consists of three shell parts representing the cage, the plate and the ring. The plate and cage parts were considered as fixed, non-deformable bodies and were represented by their contact surfaces with the ring. For the ring, fully integrated shell elements with 5 integration points through the thickness. Elastic-plastic material model was associated to the ring elements. Only the displacement of the ring in the $(\vec{x}, \vec{y})$ plane was restricted (see Figure 2). The ring was free to displace in $\vec{z}$ direction and rotate around $\vec{x}$, $\vec{y}$ and $\vec{z}$ axis. The FE model accounts for the impacts occurring at all contact surfaces including ring - springs, ring - plate and ring - cage. The assembly includes 12 individual springs, where each spring is represented by a spring element connecting a rigid part representing the contact surface with the ring to the valve cage. All contacts in the assembly are assumed to be frictionless. Viscous contact damping (VCD) with contact damping factor equal to 20% of the critical damping is used for all contacts. The VCD can be beneficial to reduce the high-frequency oscillation of contact

This is the accpted version of paper published at GL2022
http://dx.doi.org/10.18462/iir.gl2022.0155

forces in crash or impact simulations. The effects of contact damping in FEM on the total force and displacement of the ring computed at the centre of the ring was found to be negligible. However, the contact damping was found to proportionally reduce the impact force computed at the impact contact areas as compared to elastic contact (without damping). This indicates that care must be taken when interpreting the contact impact forces.

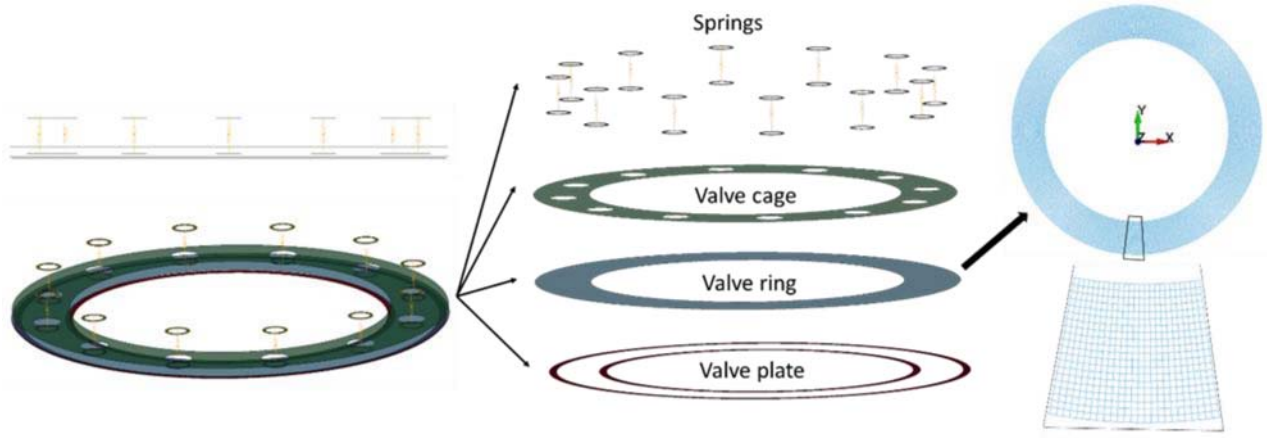

Figure 2: Discharge valve assembly as represented by the FE model with a zoomed section on the ring part showing the FE mesh.

2.2. Computational Fluid Dynamics (CFD)

The governing equations in the CFD simulations considered here are the compressible Navier-Stokes equations on a moving computational mesh, where the ring plate and other solid bodies are represented as boundaries in the mesh. The conservation equations are

$$\frac{\partial \rho}{\partial t} + \frac{\partial}{\partial x_j}\left[\rho u_j\right] = 0 \tag{1}$$

$$\frac{\partial}{\partial t}(\rho u_i) + \frac{\partial}{\partial x_j}\left[\rho u_i u_j + p\delta_{ij} - \tau_{ji}\right] = 0, \quad i = 1,2,3 \tag{2}$$

$$\frac{\partial}{\partial t}(\rho e_0) + \frac{\partial}{\partial x_j}\left[\rho u_j e_0 + u_j p + q_j - u_i \tau_{ij}\right] = 0 \tag{3}$$

where u_i are the velocity components, ρ is the density, p is the pressure, τ_{ij} are the components of the stress tensor, e_0 is the specific enthalpy and q is the heat flux. A thermodynamic Equation of State is required to close this system, and a turbulence model is also included using the Reynolds-averaging procedure and with additional transport equations for the turbulence quantities. Here we use the cubic Peng-Robinson EoS together with a Sutherland viscosity model and JANAF polynomials for heat capacity, all fitted to represent ammonia gas. For turbulence the k-omega SST model is employed. The OpenFOAM software v.1912 was used for the computations, employing a custom solver based on the existing "rhoPimpleFoam" which has dynamic mesh capability. This solver uses a pressure-based formulation that is developed for low Mach number flows, but with extensions to handle transonic situations.

In the OpenFOAM simulations, the ring plate is represented as a hole in the computational mesh, which can move according to the specified displacement. At a given point in time, the ring plate position is updated, and the resulting gas flow and pressure are computed. Using the pressure and flow conditions at the ring plate boundary, the total aerodynamic forces acting on the ring plate are computed. This is given as a linear force acting on the centre-of-mass, as well as a torque acting around the centre-of-mass of the plate. The aerodynamic forces include the pressure forces as well as viscous forces. For the present simulations, the viscous forces (drag) acting on the plate were found to be at least three orders of magnitude smaller than the pressure forces.

This is the accpted version of the paper published at GL2022
http://dx.doi.org/10.18462/iir.gl2022.0155

An illustration of the computational mesh is given in Figure 3 showing a slice through the mesh on the left-hand side, with the ring plate highlighted in green. In this illustration the domain is shown to include the cylinder space where the gas is compressed before it discharges through the valve. In that case, there is no specification of an inlet velocity in the domain, but the gas flow is driven by the piston motion represented by motion of the bottom boundary in the mesh, as shown again in Figure 3 (bottom right). As indicated in Figure 3 (top right), simulations were also performed using the simpler approach of a pressure-velocity inlet boundary condition below the ring plate, using experimentally determined pressure. A significant difference was found between these two approaches, especially as the valve is returning to the closed position. This is because the velocity field has very little room to develop properly after the inlet condition, and because the uncertainty in experimental measurements becomes large when the piston is close to top-dead center.

The simulation is run by evolving the pressure and velocity field inside the cylinder, where the gas can flow around the ring plate and escape to the outlets in the geometry shown as blue patches. In this geometry we emphasize that there are two different mesh motions occurring in different regions. Around the ring plate, the mesh motion is combined with layer addition and removal to allow the plate full freedom to travel from bottom to top and back again, removing and adding cells in the mesh. Inside the cylinder space, the mesh motion is a linear deformation such that the cells adjacent to the top are fixed, the cells adjacent to the piston are moving with a prescribed piston velocity, and the motion of cells between these two endpoints are linearly interpolated. Note that the lower outer annulus attached to the cylinder region does not move nor deform; this space represents the suction valve dead volume. Care has been taken to match the total dead volume as well as the piston clearance at top dead centre with the real geometry, but the geometric details are simplified from the real compressor.

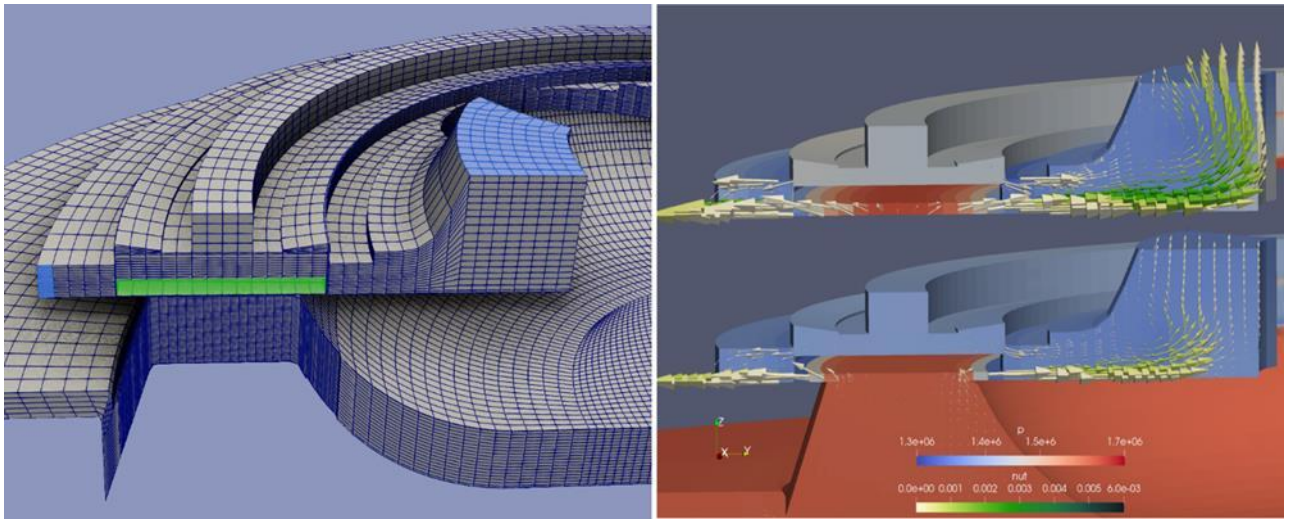

Figure 3: Cross-section of the computational mesh with ring plate highlighted in green (left), velocity field at 0.5 ms after valve opening for simulation with pressure inlet (top right) and with piston and cylinder (bottom right).

2.3. The proposed method of coupling CFD and FEM

In the simulation of the discharge valve opening, the state of the gas inside the cylinder (pressure, temperature, and flow pattern) needs to be specified at the point where the cylinder pressure is equal to the discharge pressure. To obtain this state, a precursor simulation is run where the piston starts at top-dead-centre and the pressure is equal to discharge pressure, and all valves are closed. The simulation is run until the pressure has reduced such that the suction valve should open. At that point, the simulation is stopped and the boundary condition on the suction valve annulus segment is changed to an inlet corresponding to the suction pressure. The simulation is then run again until the point where the suction valve should close. The boundary condition on the suction valve is changed back to the wall boundary condition, and the simulation is run again until the pressure in the cylinder equals the discharge pressure. At this point, the coupled simulation can start. This is illustrated in the figure below, where blue squares indicate approximately the opening and closing of the suction valve. In the finite element simulation, an initiation

This is the accpted version of the paper published at GL2022
http://dx.doi.org/10.18462/iir.gl2022.0155

step is performed to preload the springs and apply the initial pressure differential applied on the valve ring. Then, the data exchange between FEM solver and CFD solver is started as illustrated in Figure 4.

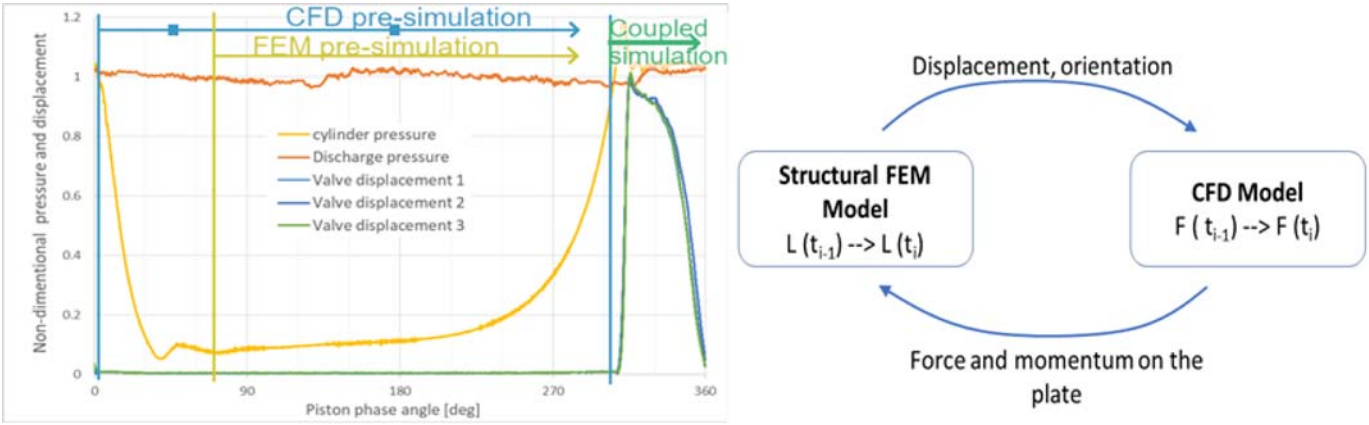

Figure 4: Left: non dimensional pressure and ring displacement as function of the piston phase angle showing the pre-simulations (initiation steps) in FEM and CFD and the coupled CFD-FEM simulations. Right: illustration of the coupling methodology with exchange of data between FEM and CFD models.

The coupling between CFD solver and FEM solver is enabled by the user-defined subroutines utilities of LS-DYNA, as well as the implementation of custom motion solvers and analysis routines in OpenFOAM. The synchronization between the two solvers is based on the use of lockfiles, which control the alternation of FEM solver and CFD solver. Two lockfiles defined to be associated to LS-DYNA and OpenFOAM respectively. These files should not exist simultaneously. Only one lockfile is present at any point in time, to indicate which solver should be running and which solver should wait for data.

The CFD-FEM coupling involves certain assumptions. The ring plate is considered as a rigid body in the CFD simulation and as a deformable body in the FE model. The amplitude of the ring deformation is small compared to the ring displacement, such that the CFD solver does not make any appreciable error by compute the flow field and pressure using an undeformed plate. Only the aerodynamic forces and torques are computed in OpenFOAM, and the effects of springs and contact impacts on the valve motion is considered through the motion transferred from FE model to CFD model.

3. RESULTS

3.1. Experimental measurements from a Mycom compressor

In order to obtain quantitative information about the motion of a ring plate valve during real compressor operations, a Mycom M-series compressor was instrumented, and measurements were taken using ammonia refrigerant at representative conditions (-15℃ evaporating temperature, 35 ℃ condensing temperature, and 1500 RPM). Pressure measurements were taken in the cylinder and the discharge chamber using Kulite XTME-190L-500A transducers. Three AEC PU-05 eddy current sensors were used to measure the valve ring displacement during actuation. All sensors were carefully protected from the detrimental influence of the ammonia atmosphere.

The obtained measurements from one cycle of the piston are shown in

Figure 5, where the non-dimensional pressure and displacement are plotted against piston phase angle. The pressure was normalized by the average discharge pressure and the displacement was normalized by the maximum lift. The valve is seen to open rapidly as the cylinder pressure exceeds the discharge pressure. It stays open until the piston passes the top dead center, then it is closed. The displacement of the ring measured by the three sensors exhibit very little deviation indicating that the ring remains flat during this cycle.

This is the accpted version of the paper published at GL2022
http://dx.doi.org/10.18462/iir.gl2022.0155

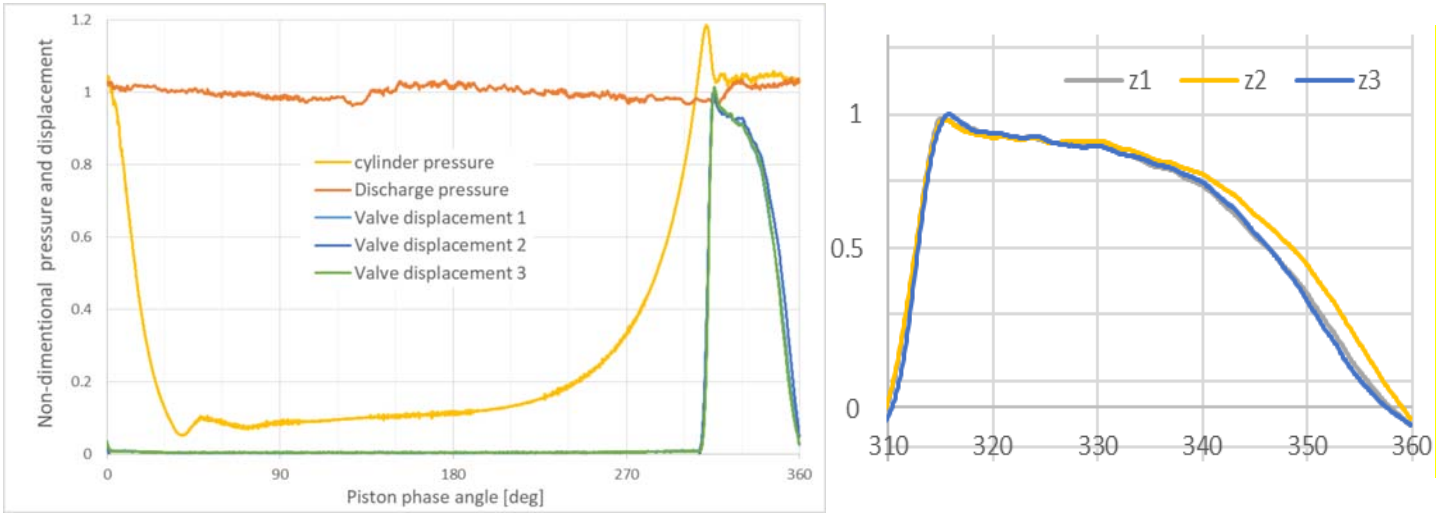

Figure 5: Measured values of cylinder pressure, discharge pressure and valve displacement at working conditions. Left: one full cycle of the piston. Right: zoom-in of the discharge valve opening and closing.

3.2. Results from CFD-FEM coupled simulations

The results from CFD-FEM coupled simulations presented here concerns first of all with investigation of the effect of considering the flow in the cylinder versus imposing inlet conditions below the ring plate, and second of all the effect of pressure inhomogeneity on the valve motion implemented through a reduced cross-section of the flow outlet on one side of the geometry.

To investigate the effect of the inlet condition, the CFD-FEM simulation was performed for two cases. The first of these, Case A, uses velocity inlet boundary condition below the ring plate, while the second, namely Case B, accounts for the gas flow inside the cylinder. In Figure 6, the forces, and the displacements at the centre of the valve ring was computed for each case. The forces are normalized by the maximum positive force in case A, corresponding to the maximum gas force opening the valve initially, while the displacement is normalized by the maximum valve lift. As can be observed, the modelling of the flow inside the cylinder in Case B gives results more consistent with the experimental observations, in that a small mechanical impact can be seen both at opening and closing of the valve. For Case A, the flow at valve closing becomes ill-posed since the velocity inlet condition must go to zero exactly at the moment of closing. Figure 7 shows that when the piston passes top dead centre, there is a certain reversed flow that occurs before the valve can close

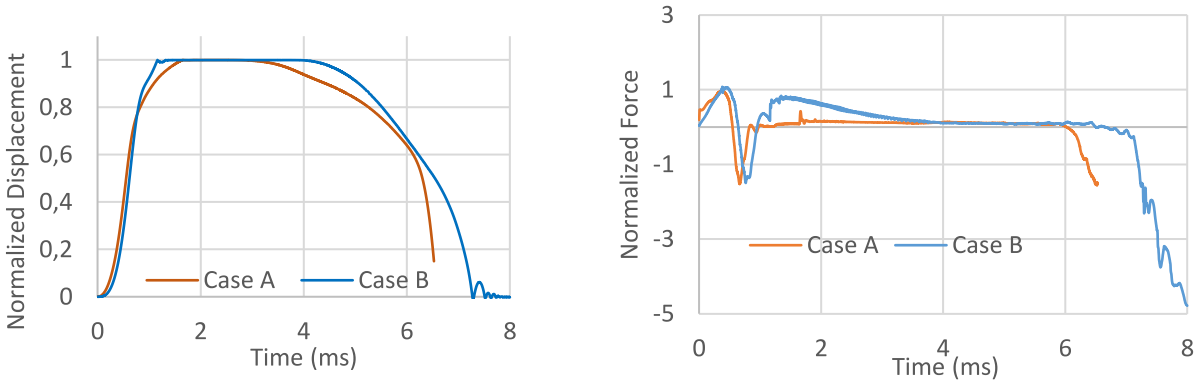

Figure 6: Displacement (left) and forces (right) for the case using velocity inlet condition versus the case including the flow inside the cylinder.

completely. This effect cannot be modelled using an imposed inlet condition, since the magnitude of the reverse flow is strongly dependent on the ring plate displacement, which is unknown before running the

This is the accpted version of the paper published at GL2022
http://dx.doi.org/10.18462/iir.gl2022.0155

simulation. In this case a substantial pressure differential is allowed to exist after valve closing. It can also be seen that the discharge flow towards the central outlet is not uniform, but rather displays a swirl pattern.

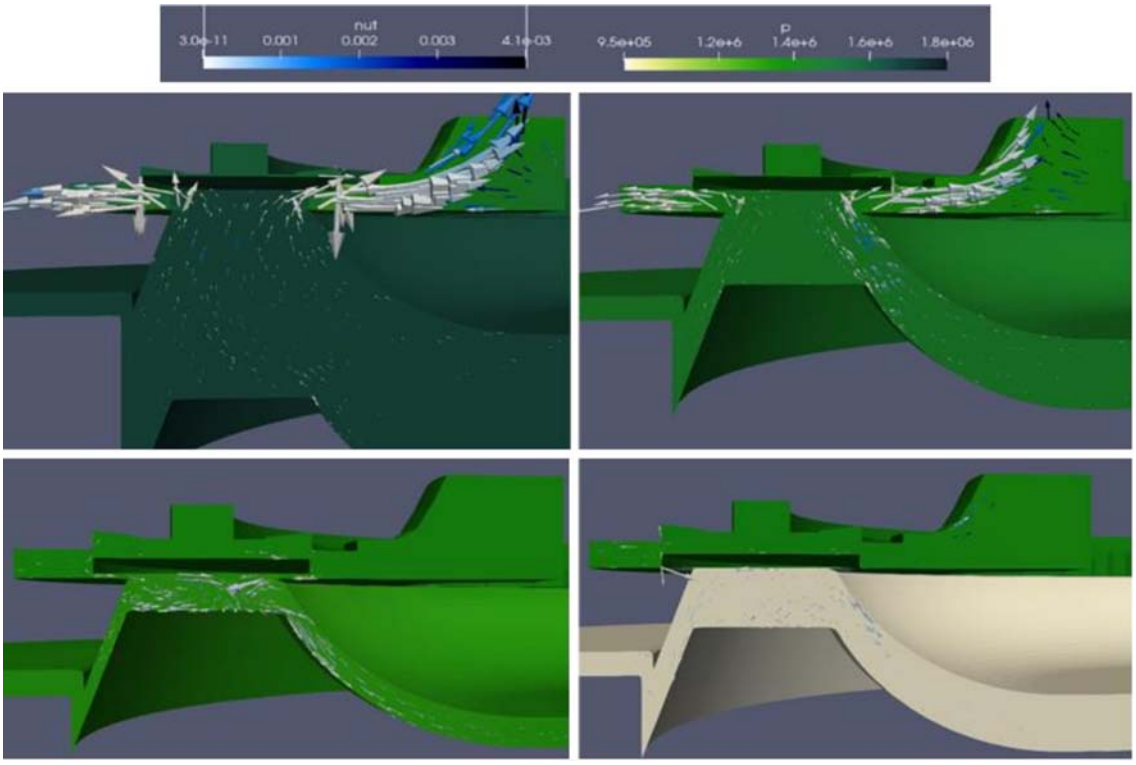

Figure 7: Snapshots of valve actuation taken at 0.5, 3.0, 7.0 and 8.0 ms after valve opening. It is seen that the valve opens quickly with strong flow into the discharge chamber when the piston is still approaching top dead center, and that the valve closes quickly after the piston passes top dead centre.

The effects of pressure inhomogeneities were studied using a geometry like in Case A that was modified to have an asymmetry in the outlet condition in the CFD. This mimics (and exaggerates) the asymmetry that can result from asymmetric configuration of the discharge chamber or of the valve cage. The results are shown in Figure 8, where on the left side, the pressure field is shown to be strongly affected by the blocking of the outlet in a region at the bottom of this figure. On the right side of the figure, the displacement dZ as well as the rotation Rx, Ry around the x- and y-axes is shown. The rotation only occurs in the direction of asymmetry, meaning that no rotary tumbling is seen here. Furthermore, the first change in rotation that is seen in the blue curve is due to the gas pressure exerting a sudden torque when the valve approaches the open condition, while the subsequent three changes in rotation are due to mechanical impacts between the valve ring and the cage. It should also be noted that the maximum lift of the centre-of-mass never reaches 1 in this case, due to the tumbling, so such tumbling can be detrimental not only to reliability but also to efficiency.

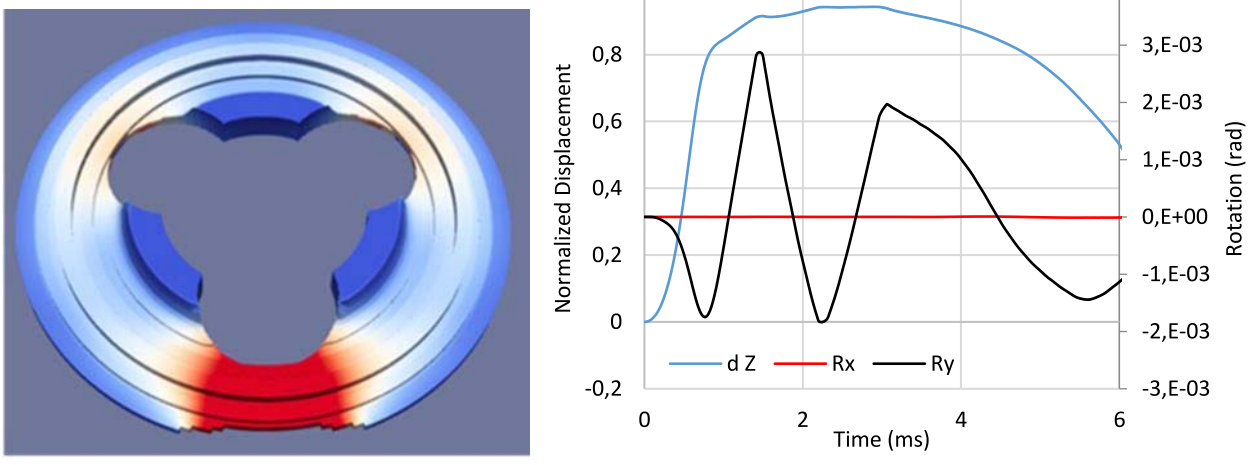

This is the accpted version of the paper published at GL2022
http://dx.doi.org/10.18462/iir.gl2022.0155

Figure 8: Setup of case with pressure inhomogeneity due to removal of a part of the outlet (left). On the right side, the resulting displacement normalised by the valve lift and the ring rotation around $\vec{x}$ and $\vec{y}$ axis.

4. CONCLUSIONS

In this paper, a coupled CFD-FEM simulation approach based on incremental interaction between the CFD and FEM solvers was developed to predict the dynamic response of the compressor. The developed approach enabled the study of detailed phenomena inside the compressor. In the present work it was demonstrated that is necessary to consider the particular aspects of the flow inside the cylinder as it exits through the valve. Using a typical inlet boundary condition to the valve cage is not able to capture the full physics of the flow. Employing a full model of the cylinder space captures in detail the reversed flow that occurs when the piston passes top dead centre, which leads to a more rapid closing of the valve, and also enables investigation of the volumetric efficiency. In all considered cases it is seen that a substantial gas damping force occurs when the valve is approaching its maximum lift, reducing the valve speed before the mechanical impact. The coupled simulation has also shown that the effect of pressure inhomogeneity in the flow field leads to a significant rotation of the valve ring, coming both from the gas damping effect and the mechanical impacts that occur subsequently, giving a lower maximum lift in terms of centre-of-mass.

ACKNOWLEDGEMENTS

The authors wish to acknowledge the financial support of the FME HighEFF Centre for Environment-friendly Energy Research funded by the Research Council of Norway and user partners (project no. 257632/E20).

REFERENCES

Adams J, Hamilton JF, Soedel W. 1974, The Prediction of Dynamic Strain in Ring Type Compressor Valves Using Experimentally Determined Strain Modes, Proc. Int. Compressor Eng. Conf., Paper 137.

Bredesen AM. 1974, Computer Simulation of Valve Dynamics as an Aid to Design, Proc. Int. Compressor Eng. Conf., Paper 117.

Cyklis P. 1994, CFD Simulation of the Flow Through Reciprocating Compressor Self-Acting Valves, Proc. Int. Compressor Eng. Conf., Paper 1016.

Elson JP, Soedel W. 1974, Simulation of the interaction of compressor valves with acoustic back pressures in long discharge lines, J. Sound Vib. 34 (2): 211–220.

Habing RA. 2005, Flow and plate motion in compressor valves, PhD Thesis, Univ. Twente.

Kim H, Ahn J, Kim D., 2008, Fluid Structure Interaction and Impact Analyses of Reciprocating Compressor Discharge Valve, Proc. Int. Compressor Eng. Conf., Paper 1936.

Lorentzen G. 1950, Leveringsgrad og virkningsgrad for kjølekompressorer, Doctoral Thesis, Norges Tekniske Høgskole.

Machu EH. 1994, The Two-Dimensional Motion of the Valve Plate of a Reciprocating Compressor Valve, Proc. Int. Compressor Eng. Conf., Paper 1012.

Palm B. 2008, Ammonia in low capacity refrigeration and heat pump systems, Int. J. Refrig. 31(4): 709–715.

Pearson A. 2008, Refrigeration with ammonia, Int. J. Refrig. 31(4): 545–551.

Ruman R, Sustek J, Tomlein P. 2015, Analysis of Pressure Losses in the Refrigeration Flow Through Reciprocating Compressor with CO2, Proc. 24th IIR Int. Congr. Refrig., Paper 124.

Tan Q, Pan S, Feng Q, Yu X, Wang Z. 2014, Fluid–Structure Interaction Model of Dynamic Behavior of the Discharge Valve in a Rotary Compressor, Proc. IMechE. J. Proc. Mech. Eng. 229(4):280-289.

Zhao B, Jia X, Sun S, Wen J, Peng X. 2018, FSI Model of Valve Motion and Pressure Pulsation for Investigating Thermodynamic Process and Internal Flow Inside a Reciprocating Compressor, Appl. Therm. Eng.

Tofique M.W, Löf A, Schillaci E, Castrillo P, Rigola J. 2021, Experimental and Numerical Analysis Of Reed Valve Movement In An Impact Fatigue Test System and Reciprocating Compressors, Proc. Int. Compressor Eng. Conf., Paper 2697.

Ervik Å, Saai A, Berstad T, Meyer O, Tsuji T, Oku T, Hattori K, Yamada K, Delhaye V, Nekså P. 2021, Modelling the dynamics of ring plate valves in reciprocating compressors using coupled CFD-FEM simulations. 10th Int. Conf. Compressors Coolants, Paper 0402.